Multiphoton L-shell ionization of H_2S using intense x-ray pulses from a free-electron laser

B. F. Murphy,[1,3,*] L. Fang,[1,3] M.-H. Chen,[2] J. D. Bozek,[3] E. Kukk,[4] E. P. Kanter,[5] M. Messerschmidt,[3] T. Osipov,[1,3] and N. Berrah[1]

[1]*Western Michigan University, 1903 West Michigan Avenue, Kalamazoo, Michigan 49008, USA*
[2]*Lawrence Livermore National Laboratory, 7000 East Avenue, Livermore, California 94550, USA*
[3]*SLAC National Accelerator Laboratory, 2575 Sand Hill Road, Menlo Park, California 94025, USA*
[4]*Department of Physics and Astronomy, University of Turku, FI-20014, Turku, Finland*
[5]*Argonne National Laboratory, 9700 South Cass Avenue, Lemont, Illinois 60439, USA*

(Received 29 July 2012; published 29 November 2012)

Sequential multiphoton L-shell ionization of hydrogen sulfide exposed to intense femtosecond pulses of 1.25-keV x rays has been observed via photoelectron, Auger electron, and ion time-of-flight spectroscopies. Monte Carlo simulations based on relativistic Dirac-Hartree-Slater calculations of Auger decay rates in sulfur with single and double L-shell vacancies accurately model the observed spectra. While single-vacancy-only calculations are surprisingly accurate even at the high x-ray intensity used in the experiment, calculations including double-vacancy states improve on yield estimates of highly charged sulfur ions. In the most intense part of the x-ray focal volume, an average molecule absorbs more than five photons, producing multiple L-shell vacancies in 17% of photoionization events according to simulation. For 280-fs pulse duration and $\sim 10^{17}$ W cm^{-2} focal intensity, the yield of S^{13+} is $\sim$1% of the S^{3+} yield, in good agreement with simulations. An overabundance of S^{12+}, and S^{14+} observed in the experimental ion spectra is not predicted by either single-vacancy or double-vacancy calculations.

DOI: 10.1103/PhysRevA.86.053423 PACS number(s): 32.80.Aa, 32.80.Rm, 33.60.+q, 32.80.Hd

I. INTRODUCTION

The development 40 years ago of dedicated synchrotron x-ray light sources produced breakthroughs in measuring, through single-photon absorption, the internal electronic structure of atoms, ions, and molecules. Photoelectron and Auger spectroscopy, along with cross-section measurements, provided a direct test of theoretical atomic and molecular structure models, including study of L-shell ionization of H_2S [1–6]. With few exceptions (e.g., single-photon double ionization) the interactions studied are initiated by the removal of a single inner-shell electron from the target atom or molecule, followed by the subsequent refilling of this single vacancy. Due to the limits on intensity of third generation synchrotron x-ray sources, multiphoton studies in which a single atom or molecule absorbs more than one photon were beyond experimental reach.

Recently, the development of high-peak brightness x-ray free-electron lasers (FELs) such as the SLAC Linac Coherent Light Source (LCLS) [7] has enabled the study of nonlinear processes in atoms and molecules by multiphoton spectroscopies. The first experiments [8–16] focused intense pulses of x rays onto atoms and molecules from the first row of the periodic table, producing multiple K-shell vacancies that alter the behavior of the target atom or molecule. In neon, high-intensity exposure to 100-fs x-ray pulses led to the production of excess Ne^{9+}, which was attributed to direct two-photon absorption along with ionization out of transient excited states [8]. Because the K shell holds only two electrons, the cross section for absorption of a second photon by a single inner-shell hole (SISH) atom is reduced until the hole fills by Auger decay. In neon and nitrogen, it was observed that x-ray pulse durations comparable to the Auger decay time ($\sim$10 fs) limit the overall ion charge state production [9,10]. When a second photon is absorbed within the Auger decay time, producing a double inner-shell hole (DISH,) the binding energy of the remaining electrons is altered, changing the photoelectron and Auger spectra [11,12]. The ability to produce multiple inner-shell vacancies in significant abundance with x rays is fundamentally new, due to the unprecedented brightness of x-ray FELs.

In this work, we describe the interaction of intense 280-fs pulses of 1.25-keV x rays with H_2S molecules, resulting in sequential multiphoton L-shell ionization of sulfur ions in which DISHs play a significant role. As the sulfur compound with the simplest inner-shell electronic structure, H_2S is an ideal system in which to model multiphoton L-shell dynamics of sulfur-containing molecules. Furthermore it serves as a model of open-shell atom dynamics which may differ substantially from closed-shell systems (e.g., noble gases) in decay rates. The choice of 1.2–1.3-keV photon energy was initially made to investigate the production of H_2S 1s vacancies by simultaneous x-ray two-photon photoionization [8], which would be evident through the production of KLL Auger electrons; however, no electrons were observed in the 2.0–2.1-keV kinetic energy range of the main H_2S KLL Auger peaks [3]. Because the sulfur L-shell electron binding energy remains below 1.25 keV even for S^{13+}, the electron spectra and ion charge state distributions we observe are predominantly driven by L-shell photoionization and subsequent relaxation of L-shell holes.

In contrast to the first-row K-shell excitation experiments described above, relaxation of L-shell hole states involves many more decay paths following creation of an L-shell vacancy. Vacancies in the 2s shell fill very rapidly by Coster-Kronig (CK) decay involving the creation of a 2p vacancy, which subsequently relaxes by LMM Auger decay as

*Corresponding author: bmurphy@slac.stanford.edu

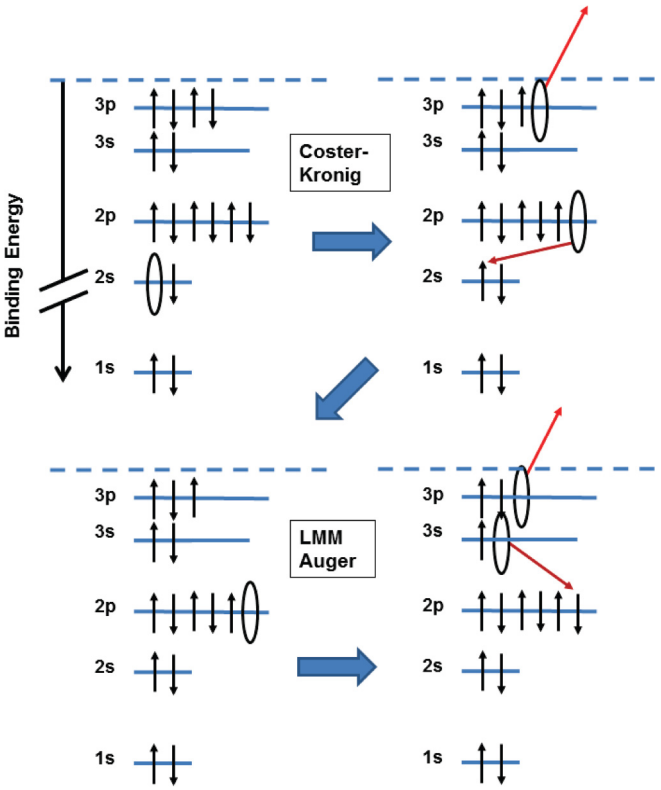

FIG. 1. (Color online) Schematic of 2*s* initial vacancy filling by Coster-Kronig (CK) decay. The CK transition proceeds rapidly (less than 1 fs), producing a longer-lived 2*p* vacancy, which then fills by *LMM* Auger decay.

shown in Fig. 1. Although in principle three or more *L*-shell vacancies could be produced in an atom under sufficiently high x-ray intensity, in this work only single and double *L*-shell vacancies are considered. DISH states exhibit enhanced rates of Auger and CK decay and increased Auger electron kinetic energy, along with reduced photoelectron kinetic energy due to increased binding potential. The increased Auger rates rapidly refill the *L* shell from the valence, producing more ions up to S^{6+} than would otherwise be observed. Above S^{6+}, Auger channels are not available, and further ionization proceeds only by photoabsorption. Auger, photoelectron, and ion charge state spectra therefore allow observation of *L*-shell DISH effects in H_2S.

II. EXPERIMENTAL METHOD

The experiment was conducted using the High-Field Physics End-Station in the Atomic, Molecular, and Optical Science hutch at the LCLS FEL. This instrument consists of an ion time-of-flight (iTOF) spectrometer and five angle-resolved electron time-of-flight (eTOF) spectrometers, described in detail elsewhere [9–12,17]. The x rays are focused to a $\sim$2-μm^2 spot by a pair of Kirkpatrick-Baez mirrors. The intensity of the focused x rays was varied from $\sim 10^{16}$ to $\sim 2 \times 10^{17}$ W cm^{-2} in order to observe intensity-dependent effects. A skimmed molecular jet mounted perpendicular to the FEL beam path delivers the target gas to the x-ray focus. Photon energies of 1.2–1.3 keV were used in the experiment. Although the FEL pulse contains $\sim$0.1% third harmonic content, this component is rejected by the transport and focusing mirrors, and is estimated to be negligible in the focus when the photon energy is above 1 keV.

Electron spectrometers are aligned both in the dipole plane (along the FEL polarization axis) and out of the dipole plane, allowing photoelectrons ionized from *s*-wave states to be distinguished from *p*-wave photoelectrons and isotropically emitted Auger electrons. Retarding voltages were chosen to record photo- and Auger electron spectra at high resolution following *L*-shell excitation of sulfur, including CK electrons. To avoid space charge broadening of the electron spectra, the pressure in the target chamber was maintained below 3×10^{-8} Torr during the measurements. The count rate was held to approximately one electron per spectrometer per shot for constant fraction discrimination.

III. SIMULATION

The simulations presented here combine traditional external-field free-atomic calculations with a statistical model of photoionization and Auger decay driven by an x-ray pulse of a given photon energy, spatial distribution, and temporal pulse structure. We assume that the state of a sulfur ion on any given time step is well described by a static electronic configuration, and that the transitions between states occur faster than the smallest time step considered. Our experimental data include contributions from the low-intensity region around the FEL focus as well as the high-intensity focal volume, so comparisons with simulation are feasible only after averaging over the intensity distribution. Secondary interactions of photo- and Auger electrons with the target molecules are ignored. The FEL intensity distribution in the interaction region is modeled as a radially symmetric Gaussian profile corresponding to the measured focal spot. Because the Rayleigh range of the FEL focus is long compared to the spectrometer acceptance window, a uniform intensity along the FEL axis is assumed. Monte Carlo simulations at 28 intensity values are weighted in proportion to their contribution to the FEL intensity distribution and combined as intensity-integrated ion and electron spectra.

Because there is no correlation between the pulse energy and H^+ ion kinetic energy we measure, we know that the H atoms dissociate rapidly from the S atom as ionization proceeds. Therefore it is appropriate to treat the target as a sulfur ion and ignore the hydrogen when predicting contributions to Auger and photoelectron spectra from charge states above S^{2+}. At the 1.2–1.3-keV x-ray photon energy used in our experiments, photoabsorption by hydrogen atoms is negligible. Treating only the S ions greatly simplifies the modeling of both photoionization and Auger decay. Binding energies and cross sections for photoionization of S^{1+} to S^{13+} ions in various ($1s_{1/2}$, $2s_{1/2}$, $2p_{1/2}$, $2p_{3/2}$, $3s_{1/2}$, $3p_{1/2}$, $3p_{3/2}$, $4s_{1/2}$, $4p_{1/2}$, $4p_{3/2}$, $5s_{1/2}$) electronic configurations, including ionization from SISH states to form DISH states, are calculated using the Hartree-Fock method [18]. Auger energies and Auger rates are calculated using the relativistic Dirac-Hartree-Slater model with relaxation, and include Coulomb, generalized Breit, and QED energies. Contributions from the dominant 4*s*, 4*p*, 5*s* shake-up (SU) and shake-off (SO) electron correlation

channels are included in the photoionization model, and Auger decay of these shake-up states is included in the relaxation model.

Dynamics of the x-ray pulse interaction with H_2S molecules are modeled using a Monte Carlo simulation of L-shell and M-shell dynamics of sulfur ions. The x-ray pulse is represented as a random set of "spikes" of photon intensity, with spike duration matching the ∼1-fs FEL coherence length, pulse duration matching the measured electron bunch duration (280 fs) at the undulator exit, and photon number matching the measured pulse energy. Photoionization proceeds by random events based on the instantaneous photon intensity and calculated photoabsorption cross sections corrected for the specific electronic configuration of the atom during that time step. When a core vacancy exists on a given time step, Auger decay occurs through channels and rates calculated for the specific electronic configuration. Though photoionization turns off at 280 fs, the simulation continues for 1000 fs to allow decay of electronic configurations with low Auger rates. Using 50-as time steps, the maximum probability of photoionization on a given time step is less than 1%. The maximum probability of CK decay on a given time step is 14%, while the maximum probability for normal (LMM) Auger decay is less than 1%. X-ray fluorescence accounts for less than 1% of all hole-filling events, and is therefore not included in the model.

IV. IONS: SPECTRA AND MODEL

Highly charged sulfur ions above S^{6+} are produced by the FEL pulse for pulse energies over 0.25 mJ as measured before the FEL transport and focusing optics. The transmission of the five optical surfaces and numerous apertures, which was initially unknown, is estimated to be ∼30% based on comparison between ion yield simulations and measurements. Ion time-of-flight spectra versus (mirror transmission corrected) pulse energy are plotted in Fig. 2. The peak corresponding to S^{1+} is broadened by contributions from H_2S^+ and HS^+ fragments, while the S^{2+} peak has a sharp shoulder corresponding to H_2S^{2+}, with almost no HS^{2+} evident. No molecular fragment ions are observed with charge greater than 2+. In Fig. 3, the ion yield is calculated by integrating the iTOF signals around the S^{n+} ion peaks and assuming that the multi-channel plate (MCP) response is equal for all charge states. Integration boundaries include the "major" ion peaks as well as their associated molecular fragments. Simulated and measured ion yields are normalized to the S^{3+} yield. The observed yield of S^{1+} and S^{2+} is substantially higher than predicted by simulations, possibly due to molecular dissociation channels which are not included in the model. For charge states above 3+, simulations largely agree with the observed ion yields over an order of magnitude range of x-ray pulse energy. Integrated-ion yields versus pulse energy show better agreement with a model including DISH and SISH Auger rates than with a model including only SISH rates. While the DISH and SISH-only models agree at low intensities where DISH states are rare, at high intensities the model including DISH calculations more accurately predicts the appearance of highly charged sulfur ions. The DISH model fit is optimal for a photon transmission of 28%, while the SISH-only model is optimal at 30% mirror transmission. The strong signals at S^{12+} and S^{14+} which appear at pulse energies >0.25 mJ and are not fit well by the model may be due to O^{6+} and O^{7+} produced by a small amount of residual water in the interaction region.

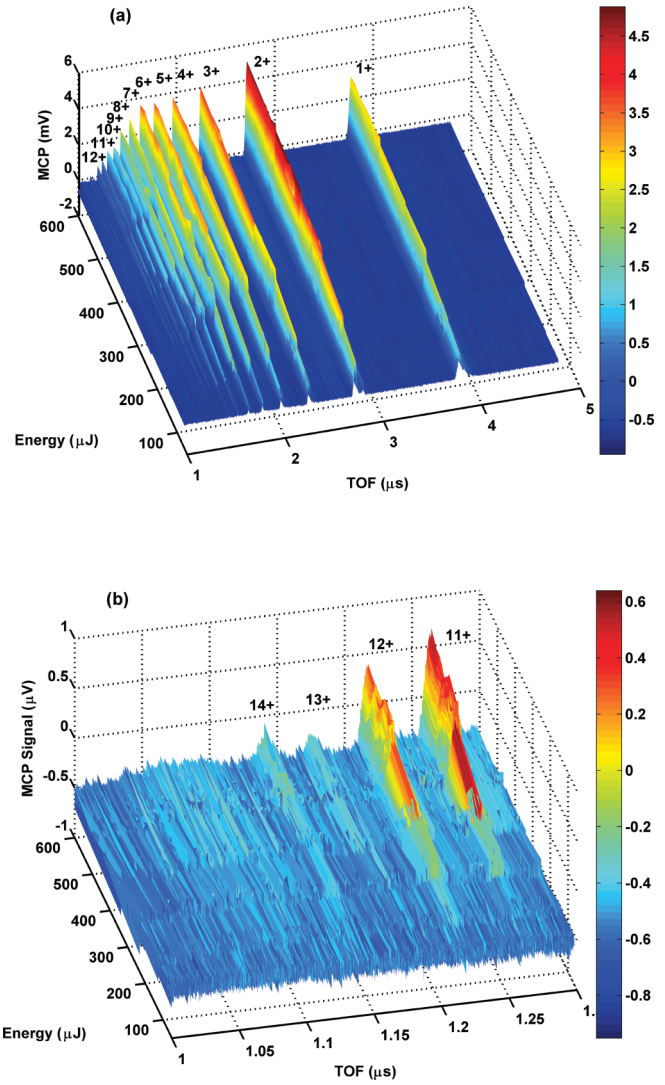

FIG. 2. (Color online) Ion time-of-flight MCP signal from H_2S versus transmission-corrected x-ray pulse energy. (a) Ion charge states from S^{1+} to S^{14+} are observed, with higher charge states appearing as the x-ray intensity increases. (b) For x-ray pulse energies over 500 μJ, S^{11-14+} ions are observed.

V. PHOTOELECTRONS: SPECTRA AND MODEL

Photoelectron spectra acquired using three dipole and one nondipole plane spectrometer are presented in Fig. 4, along with simulated spectra from the Monte Carlo model. Simulations are normalized to measured data using the $2p$ peak. The broader acceptance of the eTOFs compared to the iTOF results in averaging over a larger volume at low intensity; simulations run at 550 μJ, while in good agreement with respect to ion yield spectra, predict far more ion and inner-shell hole peaks than we observe in the electron spectra. However,

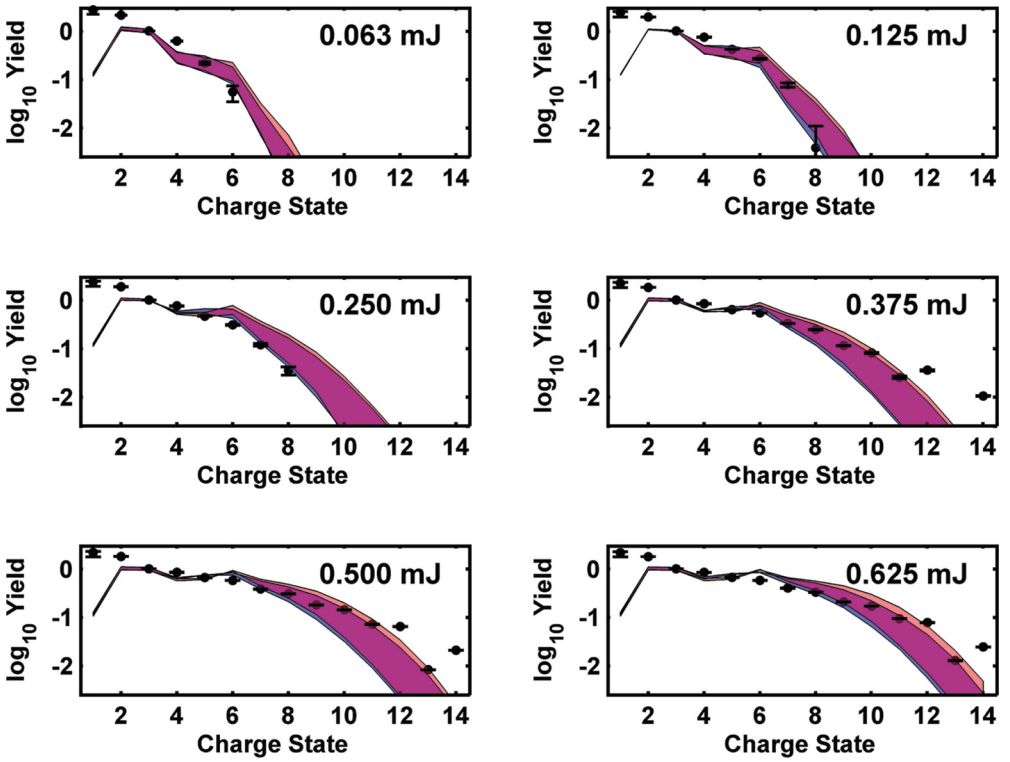

FIG. 3. (Color online) Ion yield versus simulation, normalized to S^{3+} yield. Data (black diamonds) were acquired by varying the FEL pulse energy between 63 and 625 μJ in the interaction region, and integrating over energy variation of $\pm 30\%$ at each energy step. Simulations were performed considering only single L-shell vacancy Auger calculations (blue band) and both single- and double-vacancy calculations light red band (light grey) with major shake-up/off channels in both cases. Overlap in simulations is shown in purple. Simulations show the ion yield predicted for Gaussian profile x-ray pulses within $\pm 30\%$ of the central energy.

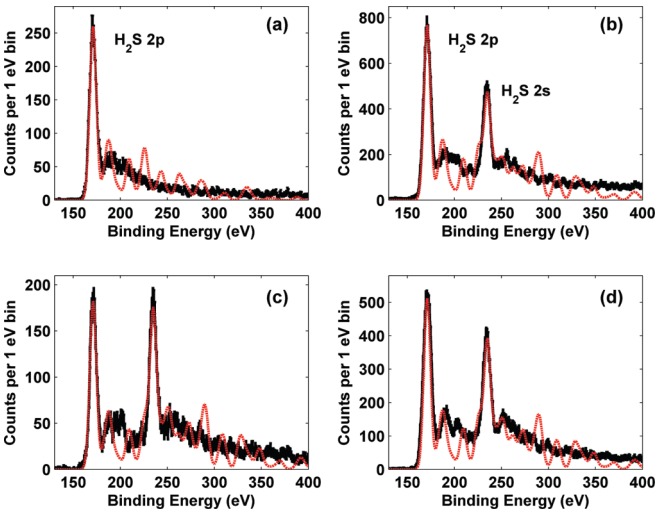

FIG. 4. (Color online) Angle-resolved H_2S photoelectron spectrum compared to simulation. Spectrometer angles are (a) nondipole plane, (b) magic angle with respect to FEL polarization axis, (c) along FEL polarization axis,(d) magic angle with respect to FEL propagation axis. Data (black line) were acquired at 550 $\pm$ 50 μJ pulse energy. DISH calculations at 375 μJ pulse energy (red dashed line; see text for explanation) were convolved with a 10-eV width Gaussian function representing the photon bandwidth and centroid jitter of the FEL photon energy.

simulations run at 375 μJ show substantial agreement with the major peaks of the measured spectra. The atomic model simulation predicts more distinct peaks resulting from ion charge states than we observe in the data. For the lowest charge states this is likely due to the limitations of describing molecular photoelectron spectra using a purely atomic model; the broadening of electron peaks associated with higher ion charge states may be due to volume space charge effects in the interaction region. Though the simulations show strong peaks not observed in the measured spectra, the average electron intensities are consistent across all spectra when considering a window of 10–15 eV width.

Angle-resolved spectrometry separates $2p$ and $2s$ contributions and allows calculation of the photoemission asymmetry parameter. Electron spectrometers mounted in the nondipole plane do not receive photoelectrons from states with s-wave symmetry, while all electron spectrometers receive photoelectrons from states with p-wave symmetry. Taking into account overlap of spectra due to ion contributions, the ratio of $2s/2p$ peak amplitudes is 0.9 along the FEL polarization axis, 0.65 at the 54.7° magic angle with respect to the FEL polarization axis, and 0.54 at the magic angle with respect to the FEL propagation axis. The angular distributions predicted by simulation, which depend only on the ratio of emitted $2s$ and $2p$ electrons, are in good agreement with the observed $2s/2p$ ratios in Fig. 4. In Fig. 5 measured data from the nondipole plane

TABLE I. Peak assignments for H_2S photoelectron spectrum. Contributions from correlated electron shake-up (SU) and shake-off (SO), as well as ionization from states with an initial inner-shell hole (ISH) or double inner-shell hole (DISH) are noted along with the charge state and parent molecule or atom.

Binding energy (eV)	Label	Description
192	A	H_2S $2p$ SU, S^{1+} $2p$
204	B	H_2S $2p$ SU, S^{2+} $2p$
218	C	S^{1+} DISH $2p$
254	D	H_2S $2s$ SU/SO, S^{3+} $2p$
264	E	S^{1+} $2s$, S^{5+} $2p$
279	F	S^{2+} $2s$, S^{1+} ISH $2s$
283	G	S^{6+} $2p$, S^{1+} ISH $2s$
294	H	S^{3+} $2s$, S^{5+} $2p$
303	I	S^{4+} $2s$
317	J	S^{6+} $2p$, S^{3+} ISH $2s$
335	K	S^{6+} $2s$, S^{7+} $2p$
357	L	S^{7+} $2p$

eTOF is plotted along with the average of the three dipole plane eTOFs to illustrate the angular dependency of features in the spectrum. Contributions from multiple charge states and electronic configurations make the photoelectron structure complex. Distinct peaks due to several ionic states and one DISH-related feature are observed and listed in Table I.

VI. AUGER ELECTRONS: SPECTRA AND MODEL

Auger electron spectra, acquired using a nondipole plane electron time-of-flight spectrometer, are presented in Fig. 6.

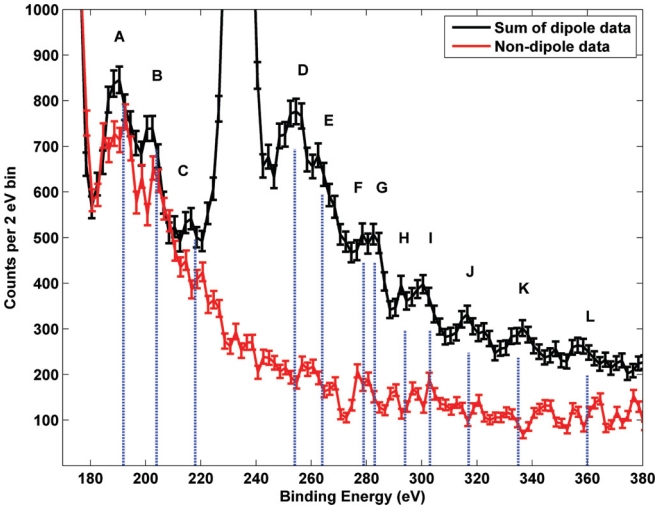

FIG. 5. (Color online) Detail of measured H_2S photoelectron spectrum near neutral H_2S $2s$ and $2p$ binding energy. Data from multiple spectrometers are combined (black, upper line) to improve statistics. Data (red line) from a nondipole plane spectrometer is plotted to help distinguish $2s$ and $2p$ features. Features A–L are identified in Table I. Feature J results from ionization of a $2p$ electron from sulfur with an L-shell vacancy. Data were acquired at 550 ± 50 μJ pulse energy. Peak markers (vertical blue lines) are from calculated binding energies of sulfur ions.

We identify two features in the *LVV* spectrum which result predominantly from DISH states as labeled. Several other features predicted by both DISH and SISH calculations are not apparent in the measured spectrum. Ion charge states up to S^{6+} contribute features down to 70 eV. The presence of a weak Auger electron peak near 500 eV (Fig. 4, inset) further suggests the presence of a small amount of oxygen in the ion yield data.

Because of the rapid refill of $2s$ vacancies by CK decay, the differences between DISH and SISH calculations are extremely small (Fig. 7.) Simulations accurately predict the features near 16 and 24 eV. The measured peak at 30 eV is broader and more energetic than the 28-eV peak predicted by simulation, though the integrated intensity is consistent with the atomic model. The measured peak at 40 eV is shifted to slightly lower energy than in simulation, with substantially more breadth and intensity. In general, the difference between the measured CK spectrum and the calculated atomic CK spectrum is larger than the difference between measured and model Auger spectra. This may result from the fact that CK electrons are primarily produced from the lowest H_2S molecular charge states, while Auger electrons are emitted for atomic ions up to S^{6+}.

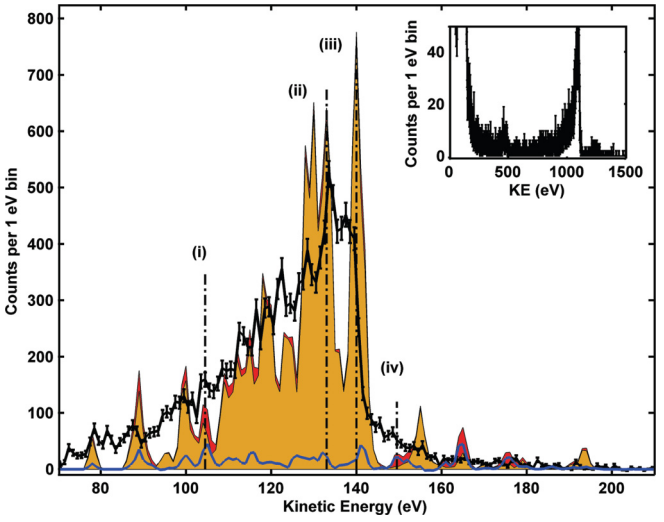

FIG. 6. (Color online) H_2S LMM Auger electron spectrum compared to simulation. This spectrometer is mounted perpendicular to both the FEL propagation axis and the FEL polarization. Data (black line) was acquired at 550 ± 50 μJ pulse energy. DISH calculations red fill (medium grey) and SISH-only calculations yellow fill (ligth grey) were run using the same pulse energy distribution as the data. The difference between the double-vacancy simulations and simulations run with only single-vacancy paths is plotted (blue line) to highlight features related to L-shell double vacancies. Features (i) and (iv) correspond to energies where simulations predict dominant DISH contributions from the S^{5+} $L_2M_2M_2$ and S^{3+} $L_2M_2M_2$ Auger lines, respectively. The dominant features (ii) and (iii) correspond to molecular H_2S^+ $L_2M_2M_2$ and S^{3+} $L_2M_2M_2$ Auger decay, respectively. Inset: H_2S nondipole plane high energy electron spectrum. Sulfur valence and $2p$ photoelectrons are apparent near 1250 and 1100 eV, respectively. Auger electrons from a small amount of oxygen present in the interaction volume (likely as H_20) are visible as a broad peak just below 500 eV.

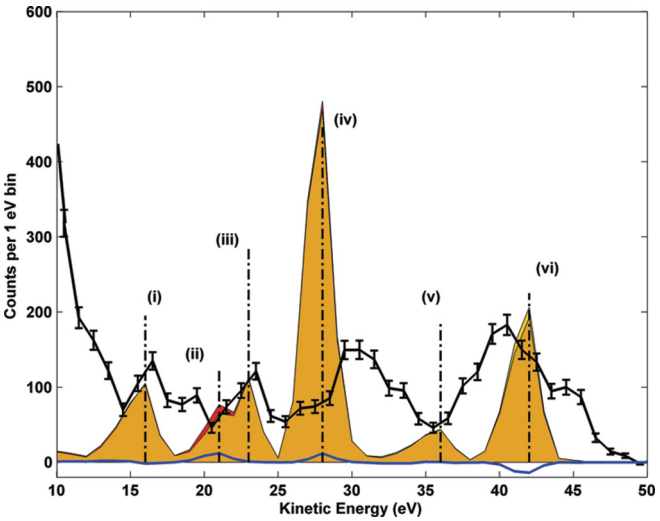

FIG. 7. (Color online) H_2S CK electron spectrum compared to simulation. Calculated transitions are labeled (i)–(vi): (i) 16 eV S^{3+} $L_1L_3M_{1,2,3}$ (ii) 21 eV S^{1+} $L_1L_2M_1$ shake-up, (iii) 23 eV S^{1+} $L_1L_3M_1$ shake-up, (iv) 28 eV S^{1+} $L_1L_{2,3}M_1$, (v) 36 eV S^{1+} $L_1L_{2,3}M_{2,3}$ shake-up, (vi) 42 eVS^{1+} $L_1L_{2,3}M_{2,3}$. Data (black line) were acquired at 550 $\pm$ 50 μJ pulse energy. DISH calculations red fill (medium grey) and SISH-only calculations yellow fill (light grey) were run at 375 μJ pulse energy (see text for explanation.) The difference between the double-vacancy simulations and simulations run with only single-vacancy paths is plotted (blue line) to highlight features related to L-shell double vacancies.

VII. CONCLUSIONS

We have measured the ion yield spectrum and Auger and photoelectron spectrum of H_2S under intense ($\sim 10^{17}$ W cm^{-2} and 280-fs pulse duration) FEL x-ray exposure in a regime where multiple vacancies in the sulfur L shell are common. In the region of highest x-ray intensity an average molecule absorbs more than five photons, producing multiple L-shell vacancies in 17% of photoionization events. In comparing Monte Carlo simulations of sulfur ions under x-ray illumination with the experimental data, we find that consideration of only single L-shell vacancies produces photoelectron and Auger spectra in rough agreement with the experimental data, while consideration of both single and double vacancies better predicts the onset of highly charged sulfur ions. The inclusion of additional shake-up and shake-off channels in both the photoexcitation and Auger decay models could improve the accuracy of the atomic model presented here. Adapting this method to time-dependent molecular orbitals could facilitate modeling of molecular dynamics under intense x-ray illumination. As x-ray FEL facilities continue to improve performance and peak intensity, the effects of multiple inner-shell vacancies on x-ray-matter interactions will be increasingly apparent. No signs of simultaneous two-photon K-shell processes (e.g., as KLL Auger electrons or S^{15+} or S^{16+}) were observed at this fluence.

ACKNOWLEDGMENTS

This work was funded by the DOE, Office of Science, Basic Energy Science, Chemical, Geosciences, and Biological Divisions. Portions of this research were carried out at the Linac Coherent Light Source at SLAC National Accelerator Laboratory. LCLS is an Office of Science User Facility operated for the US Department of Energy Office of Science by Stanford University. E.K. acknowledges the financial support of the Academy of Finland. We thank M. Hoener, B. McFarland, C. Buth, C. Blaga, C. Bostedt,, D. Rolles, E. Hosler, L. DiMauro, M. Glownia, M. Guehr, O. Gessner, O. Kornilov, V. Petrovic, P. H. Bucksbaum, J. C. Castagna, M. Steger, and all of the LCLS support staff for their assistance with this work.

[1] M. H. Chen and B. Crasemann, Phys. Rev. A **16**, 1495 (1977).
[2] H. Aksela, S. Aksela, A. Naves de Brito, G. M. Bancroft, and K. H. Tan, Phys. Rev. A **45**, 7948 (1992).
[3] L. Asplund, P. Kelfve, B. Blomster, H. Siegnahn, and K. Siegbahn, Phys. Scr. **16**, 273 (1977).
[4] A. Naves de Brito and H. Agren, Phys. Rev. A **45**, 7953 (1992).
[5] G. Turri, G. Snell, B. Langer, M. Martins, E. Kukk, S. E. Canton, R. C. Bilodeau, N. Cherepkov, J. D. Bozek, A. L. Kilcoyne, and N. Berrah, Phys. Rev. A **70**, 022515 (2004).
[6] G. Turrri, G. Snell, B. Langer, M. Martins, E. Kukk, S. E. Canton, R. C. Bilodeau, N. Cherepkov, J. D. Bozek, A. L. D. Kilcoyne, and N. Berrah, Phys. Rev. Lett. **92**, 013001 (2004).
[7] P. Emma *et al.*, Nat. Photonics **4**, 641 (2010).
[8] G. Doumy *et al.*, Phys Rev. Lett. **106**, 083002 (2011).
[9] M. Hoener *et al.*, Phys. Rev. Lett. **104**, 253002 (2010).
[10] L. Young *et al.*, Nature **466**, 56 (2010).
[11] L. Fang, M. Hoener, O. Gessner, F. Tarantelli, S. T. Pratt, O. Kornilov, C. Buth, M. Gühr, E. P. Kanter, C. Bostedt, J. D. Bozek, P. H. Bucksbaum, M. Chen, R. Coffee, J. Cryan, M. Glownia, E. Kukk, S. R. Leone, and N. Berrah, Phys. Rev. Lett. **105**, 083005 (2010).
[12] J. P. Cryan *et al.*, Phys. Rev. Lett. **105**, 083004 (2010).
[13] N. Berrah *et al.*, Proc. Natl. Acad. Sci. USA **108**, 16912 (2011).
[14] P. H. Bucksbaum, R. Coffee, and N. Berrah, Adv. At. Mol. Opt. Phys. **60**, 239, (2011).
[15] P. Salén, P. van der Meulen, H. T. Schmidt, R. D. Thomas, M. Larsson, R. Feifel, M. N. Piancastelli, L. Fang, B. Murphy, T. Osipov, N. Berrah, E. Kukk, K. Ueda, J. D. Bozek, C. Bostedt, S. Wada, R. Richter, V. Feyer, and K. C. Prince, Phys. Rev. Lett. **108**, 153003 (2012).
[16] V. S. Petrović *et al.*, Phys. Rev. Lett. **108**, 253006 (2012).
[17] J. D. Bozek, Eur. Phys. J. Spec. Top. **169**, 129 (2009).
[18] R. D. Cowan, *Theory of Atomic Spectra* (University of California Press, Berkeley, 1981).